AIP | Applied Physics Letters

Current-induced spin-orbit torque switching of perpendicularly magnetized Hf|CoFeB|MgO and Hf|CoFeB|TaOx structures

Mustafa Akyol, Guoqiang Yu, Juan G. Alzate, Pramey Upadhyaya, Xiang Li, Kin L. Wong, Ahmet Ekicibil, Pedram Khalili Amiri, and Kang L. Wang

Citation: Applied Physics Letters **106**, 162409 (2015); doi: 10.1063/1.4919108
View online: http://dx.doi.org/10.1063/1.4919108
View Table of Contents: http://scitation.aip.org/content/aip/journal/apl/106/16?ver=pdfcov
Published by the AIP Publishing

Articles you may be interested in

Effect of the oxide layer on current-induced spin-orbit torques in Hf|CoFeB|MgO and Hf|CoFeB|TaOx structures
Appl. Phys. Lett. **106**, 032406 (2015); 10.1063/1.4906352

Spin-orbit torque-driven magnetization switching and thermal effects studied in Ta\CoFeB\MgO nanowires
Appl. Phys. Lett. **105**, 122404 (2014); 10.1063/1.4896225

Current-driven perpendicular magnetization switching in Ta/CoFeB/[TaOx or MgO/TaOx] films with lateral structural asymmetry
Appl. Phys. Lett. **105**, 102411 (2014); 10.1063/1.4895735

Spin-orbit torque magnetization switching of a three-terminal perpendicular magnetic tunnel junction
Appl. Phys. Lett. **104**, 042406 (2014); 10.1063/1.4863407

Annealing temperature window for tunneling magnetoresistance and spin torque switching in CoFeB/MgO/CoFeB perpendicular magnetic tunnel junctions
J. Appl. Phys. **110**, 103915 (2011); 10.1063/1.3662893

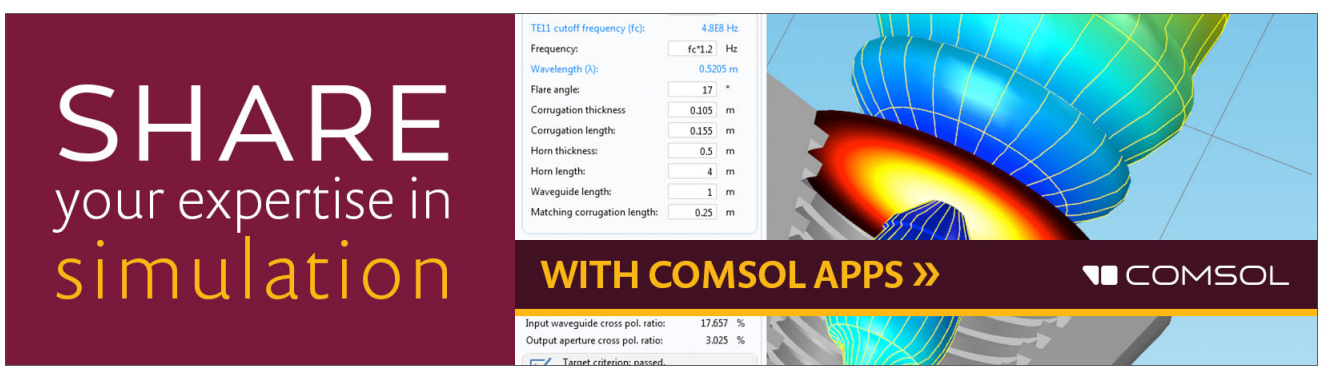

This article is copyrighted as indicated in the article. Reuse of AIP content is subject to the terms at: http://scitation.aip.org/termsconditions. Downloaded to IP: 128.97.89.222 On: Fri, 22 May 2015 17:17:30

Current-induced spin-orbit torque switching of perpendicularly magnetized Hf|CoFeB|MgO and Hf|CoFeB|TaO_x structures

Mustafa Akyol,[1,2] Guoqiang Yu,[1] Juan G. Alzate,[1] Pramey Upadhyaya,[1] Xiang Li,[1] Kin L. Wong,[1] Ahmet Ekicibil,[2] Pedram Khalili Amiri,[1] and Kang L. Wang[1]
[1]*Department of Electrical Engineering, University of California, Los Angeles, California 90095, USA*
[2]*Department of Physics, University of Çukurova, Adana 01330, Turkey*

(Received 5 March 2015; accepted 15 April 2015; published online 23 April 2015)

We study the effect of the oxide layer on current-induced perpendicular magnetization switching properties in Hf|CoFeB|MgO and Hf|CoFeB|TaO_x tri-layers. The studied structures exhibit broken in-plane inversion symmetry due to a wedged CoFeB layer, resulting in a field-like spin-orbit torque (SOT), which can be quantified by a perpendicular (out-of-plane) effective magnetic field. A clear difference in the magnitude of this effective magnetic field (H_z^{FL}) was observed between these two structures. In particular, while the current-driven deterministic perpendicular magnetic switching was observed at zero magnetic bias field in Hf|CoFeB|MgO, an external magnetic field is necessary to switch the CoFeB layer deterministically in Hf|CoFeB|TaO_x. Based on the experimental results, the SOT magnitude (H_z^{FL} per current density) in Hf|CoFeB|MgO ($-14.12\,\mathrm{Oe}/10^7\ \mathrm{A\,cm^{-2}}$) was found to be almost 13× larger than that in Hf|CoFeB|TaO_x ($-1.05\,\mathrm{Oe}/10^7\ \mathrm{A\,cm^{-2}}$). The CoFeB thickness dependence of the magnetic switching behavior, and the resulting H_z^{FL} generated by in-plane currents are also investigated in this work. © *2015 AIP Publishing LLC*.
[http://dx.doi.org/10.1063/1.4919108]

The manipulation of magnetization in thin ferromagnetic layers using an in-plane electric current, which generates spin-orbit-torque (SOT) on the magnetic moments, is being explored as an alternative way to perform writing in magnetic tunnel junctions (MTJs),[1] with improved energy efficiency, reliability, and density compared to magnetic field-based and spin-transfer torque (STT)-based methods.[2–11] The current-induced SOTs generated in heavy-metal (HM) | ferromagnet (FM) | oxide layer (OX) structures can be quantified in terms of internal effective magnetic fields acting on the magnetic moments. These SOTs have been attributed to the spin-Hall effect (SHE), the Rashba effect, or unknown mechanisms in various experiments.[8,12,13] In previous works, however, the origin of the current-induced torques generated by the spin-orbit coupling (SOC) has been mostly considered to be at the interface between the heavy metal and the ferromagnetic layer in a HM|FM|OX tri-layer. A large amount of work has been dedicated to identifying materials with large SOC to generate giant spin currents for magnetization switching. However, recent works have demonstrated that in fact both interfaces of the ferromagnetic layer may affect the field-like and damping-like SOT terms,[14] and hence contribute to the switching of the ferromagnetic layer by in-plane current.

In this work, we experimentally study the effective perpendicular magnetic field, H_z^{FL} generated by in-plane electric current in structures with broken in-plane structural symmetry, consisting of perpendicularly magnetized Hf|CoFeB(wedge)|MgO (MgO-based) and Hf|CoFeB(wedge)|TaO_x (TaO_x-based) tri-layers (see Fig. 1(a)). The experimental results show that the oxide layer in HM|FM|OX structures has a critical role in determining the torques on the magnetic moments generated by an in-plane current. In addition, we obtain magnetic switching phase diagrams for these different oxide layer samples, under different longitudinal magnetic fields H_L.

Hf(5)|$Co_{20}Fe_{60}B_{20}$(wedge)|MgO|TaO_x and Hf(5)|$Co_{20}Fe_{60}B_{20}$(wedge)|TaO_x stacks (thickness in nanometers and the composition of the CoFeB in atomic percent) were deposited on a thermally oxidized Si|SiO_2 substrate by a magnetron sputtering system. The CoFeB layer in both samples was grown in a wedge shape (i.e., with varying thickness from 0.4 to 1.6 nm across 50 mm along the wafer) along the y-axis (see Fig. 1(a)). The metal layers (Hf, CoFeB, and Ta) were deposited by using a dc power source. For the TaO_x-based sample, we oxidized a uniform 1.5 nm Ta layer under an O_2/Ar plasma. For the MgO-based sample, a 5 nm MgO layer was deposited by rf sputtering, and a TaO_x layer was then grown on top of the MgO for protection. After the deposition process, the TaO_x and MgO-based samples were annealed at 200 and 250 °C for 30 min, respectively. The films were then patterned into 20 μm × 130 μm Hall bars by photo-lithography and dry-etching techniques. All deposition processes and transport measurements were performed at room temperature.

The easy and hard-axis magnetization of the samples was measured by a Vibrating Sample Magnetometry (VSM) system to investigate the magnetic anisotropy energy. Figure 1(c) shows the effective magnetic anisotropy energy, K_{eff}, multiplied by the thickness of the CoFeB layer, t_{CoFeB}, as a function of the CoFeB thickness in Hf|CoFeB(wedge)|MgO and Hf|CoFeB(wedge)|TaO_x structures. Both samples exhibit out-of-plane anisotropy ($K_{eff} > 0$) for the thickness of CoFeB ranging from ~0.5 to ~1.5 nm, while in-plane anisotropy ($K_{eff} < 0$) was observed for thicker CoFeB films. The perpendicular magnetic anisotropy (PMA) in the

 © 2015 AIP Publishing LLC

This article is copyrighted as indicated in the article. Reuse of AIP content is subject to the terms at: http://scitation.aip.org/termsconditions. Downloaded to IP: 128.97.89.222 On: Fri, 22 May 2015 17:17:30

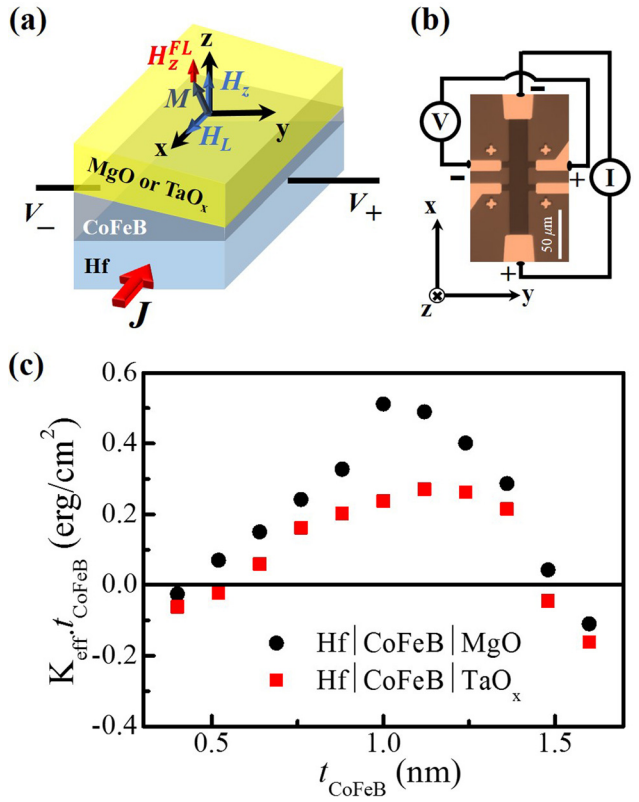

FIG. 1. (a) Schematic illustration of the film structure of Hf|CoFeB(wedge)|(MgO or TaO_x) tri-layers with electric current in the x direction. H_z and H_L represent the applied magnetic field in perpendicular and longitudinal directions to the device, respectively. H_z^{FL} corresponds to the effective field-like magnetic field in the z-direction generated by in-plane electric current due to the lateral symmetry-breaking in the device.[15] M represents the magnetization direction of the CoFeB layer, and J denotes the in-plane electric current density. (b) Optical photograph of one device and the dc experimental configuration. (c) Effective magnetic anisotropy energy, K_{eff}, multiplied by the thickness of the CoFeB film, t_{CoFeB}, as a function of the CoFeB thickness in Hf|CoFeB(wedge)|MgO and Hf|CoFeB(wedge)|TaO_x structures. Interfacial anisotropy energy density, K_i, and saturation magnetization were found to be $1.5\pm0.3\,\mathrm{erg/cm^2}$, $1.2\pm0.3\,\mathrm{erg/cm^2}$, and 1210, 1170 emu/cm^3 in MgO and TaO_x-based samples, respectively.

MgO-based sample is stronger than that in TaO_x-based structures, as seen from Fig. 1(c). We calculated the effective magnetic anisotropy energy, K_{eff}, to determine interfacial anisotropy energy for both samples from

$$K_{eff} = K_b - 2\pi M_s^2 + \frac{K_i}{t}, \tag{1}$$

where K_b is the bulk anisotropy energy density, K_i is the interfacial anisotropy energy density, and M_s is the saturation magnetization. Based on a linear fit of the data in Fig. 1(c), we found the interfacial anisotropies to be $K_i = 1.5\pm0.3\,\mathrm{erg/cm^2}$ in MgO-based and $K_i = 1.2\pm0.3\,\mathrm{erg/cm^2}$ in TaO_x-based samples, respectively.

Next, we performed transport measurements on both samples. The charge current was applied along the x axis, and the voltage generated by the extraordinary Hall effect (EHE) was measured along the y axis (see Figs. 1(a) and 1(b) for the experimental configuration). To make a fair comparison of the spin-orbit torques, we selected similar devices from each sample in terms of the PMA properties. These two devices are referred to as device I and device II in the following, which are based on the Hf|CoFeB|MgO and Hf|CoFeB|TaO_x material stacks, respectively. Figure 2 shows the extraordinary Hall resistance, R_{EHE}, as a function of the out-of-plane magnetic field, H_z, at ±1, ±5, and ±10 mA bias current, for device I (a)–(c) and device II (d)–(f), respectively. The arrows represent the magnetization direction of the devices. When the bias current value is increased from 1 to 10 mA, the coercivity is decreased for both devices as expected. However, it is observed that while the centers of the hysteresis loops are shifted to the left (right) at positive (negative) currents for device I (Hf|CoFeB|MgO), no shift occurs for device II (Hf|CoFeB|TaO_x). The shifting of the $R_{EHE} - H_z$ curves along the easy axis indicates that there is a current-induced effective field in the z direction, H_z^{FL}, which is caused by the in-plane structural asymmetry due to the varying thickness of the CoFeB layer.[15,16] As expected, this field depends on both the direction and magnitude of the applied current.

We calculated the offset field using $H_{offset} = (H^+ - H^-)/2$, where $H^+(H^-)$ is the positive (negative) switching field at each bias current value applied from ±1 to ±10 mA. Figures 3(a) and 3(b) show H_{offset} as a function of the bias current (along the x and y-axis) for device I and device II, respectively. It is observed that the offset field in device I changes linearly with the bias current along the

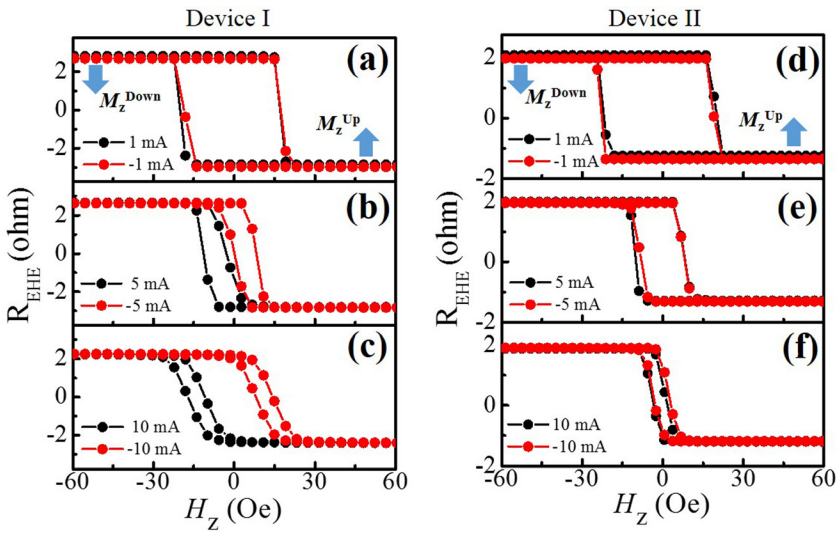

FIG. 2. Extraordinary Hall resistance (R_{EHE}) dependence on the perpendicularly applied magnetic field (H_z) at different bias current magnitudes and polarizations, for device I (a)–(c) (Hf|CoFeB|MgO) and device II (d)–(f) (Hf|CoFeB|TaO_x), respectively.

This article is copyrighted as indicated in the article. Reuse of AIP content is subject to the terms at: http://scitation.aip.org/termsconditions. Downloaded to IP: 128.97.89.222 On: Fri, 22 May 2015 17:17:30

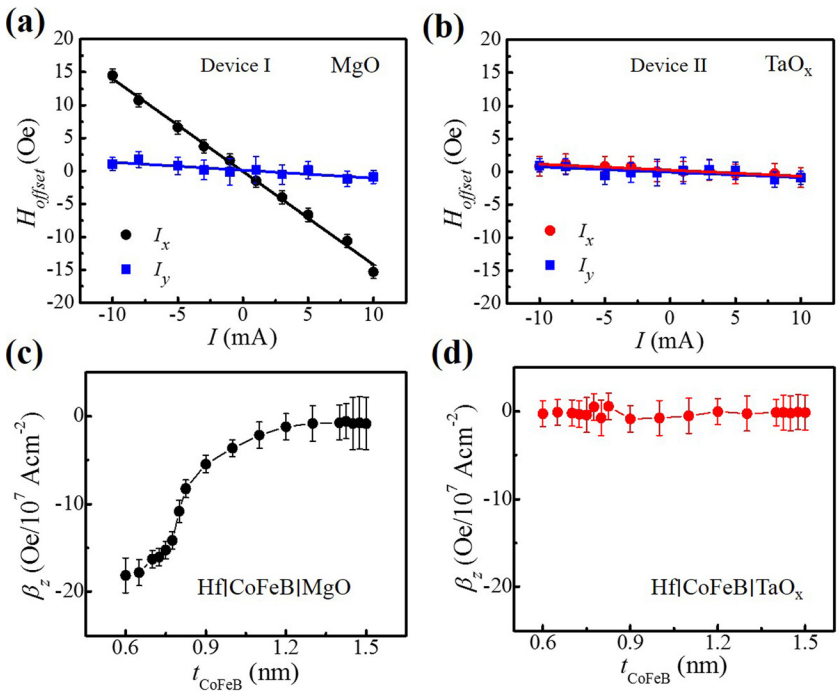

FIG. 3. (a) and (b) Offset field H_{offset} along the z axis, as a function of the bias current (I_x (I_y) is perpendicular (parallel) to the wedge) for device I on the Hf|CoFeB|MgO wafer and device II on the Hf|CoFeB|TaO_x wafer, respectively. (c) and (d) The β_z values determined using $\Delta H_{offset}/J_x$ as a function of the CoFeB thickness for both film structures.

x-axis and is much larger than the one for device II. From these results, one can then extract the offset field magnitude per current density, i.e., $\beta_z = \Delta H_{offset}/\Delta J_x$, where J_x is current density. The resulting values of β_z for devices I and II are $-14.12\,\mathrm{Oe}/10^7$ A cm^{-2} and $-1.05\,\mathrm{Oe}/10^7$ A cm^{-2}, respectively, indicating that the effective field per current density in the Hf|CoFeB|MgO structure is $\sim 13\times$ larger than in the Hf|CoFeB|TaO_x case. Figures 3(c) and 3(d) show the dependence of β_z on the CoFeB thickness along the wedge for both MgO and TaO_x-based structures. In Fig. 3(c), the magnitude of β_z decreases with the increasing of CoFeB thickness up to ~ 1.0 nm. As mentioned before, the effective magnetic anisotropy energy increases with CoFeB thickness up to this same thickness (see Fig. 1(c)). In addition, the values of β_z reduce to zero once the thickness of CoFeB goes above ~ 1.0 nm in the Hf|CoFeB(wedge)|MgO structures. In this region ($t_{CoFeB} > 1.0$ nm), the PMA decreases with increasing CoFeB thickness (see Fig. 1(c)). This behavior is consistent with results of an earlier work[16] on Ta-seeded samples with a CoFeB wedge, where in the thicker CoFeB region, the lateral symmetry breaking due to variation of anisotropy does not result in the β_z torque on magnetic moments. On the other hand, for TaO_x-based devices, the values of β_z were generally too small to observe a clear trend of the β_z dependence on CoFeB thickness (see Fig. 3(d)). In addition to applying electric current along the x-axis, which means the current is perpendicular to the wedge direction, an electric current parallel to the wedge was also applied to verify the effect of the symmetry breaking on the effective out-of-plane magnetic field generated by electric current. Figs. 3(a) and 3(b) shows the H_{offset} as a function of the bias current along the y-axis for device I (device II). It is observed that there is no significant change in the offset field by I_y in both devices, as expected due to the symmetry in this measurement configuration. We also performed all measurements on additional control samples, which do not have a wedged layer of CoFeB (i.e., no in-plane symmetry breaking) with MgO and TaO_x-capped. As expected, the current-induced out-of-plane effective magnetic field is not observed in these control samples.

It is interesting to further compare these results to the SOT-induced perpendicular magnetization switching in Ta|CoFeB(wedge)|TaO_x.[16] Although a significant H_z^{FL} has been previously observed in the case of Ta|CoFeB (wedge)|TaO_x, with its direction and magnitude both depending on the gradient of Fe oxidation at the interface, we could not observe any notable H_z^{FL} in the Hf|CoFeB(wedge)|TaO_x multilayer in this work. However, a larger value of the perpendicular current-induced effective field is observed when the oxide layer is changed, i.e., in the case of Hf|CoFeB (wedge)|MgO. It should be noted that a similar dependence of the SOTs on the oxide layer choice has recently also been observed for the conventional SOTs in non-wedged Hf|CoFeB|(MgO or TaO_x) samples.[14]

The present results (and those of Ref. 14) may have implications in terms of understanding the physical origin of the observed torques. In particular, if one assumes SHE to be the sole mechanism generating the spin-orbit torques, the latter would be expected to be proportional to the spin-Hall angle $\tau_{SHE} \sim \theta_{SH}$.[18] Hence, the SOTs generated from SHE in Ta|CoFeB|TaO_x should be expected to be larger than those in otherwise similar Hf|CoFeB|TaO_x structures, since the spin-Hall angle of Ta[1,18–20] is larger than that of Hf.[17] While this is consistent with our experimental results comparing Ta-seed devices[16] and Hf-seed devices in this work, the significant enhancement of the SOTs in Hf|CoFeB|MgO samples points to a possible additional contribution to the torque from the FM|OX interface.

Next, we performed current-driven magnetic switching in the perpendicularly magnetized devices with Hf|CoFeB| (MgO or TaO_x) stacks. Figures 4(a) and 4(b) show the out-of-plane magnetization, M_z (normalized using the extraordinary Hall resistance values), as a function of the current density, without an external magnetic field in Hf|CoFeB| MgO (Fig.

This article is copyrighted as indicated in the article. Reuse of AIP content is subject to the terms at: http://scitation.aip.org/termsconditions. Downloaded to IP: 128.97.89.222 On: Fri, 22 May 2015 17:17:30

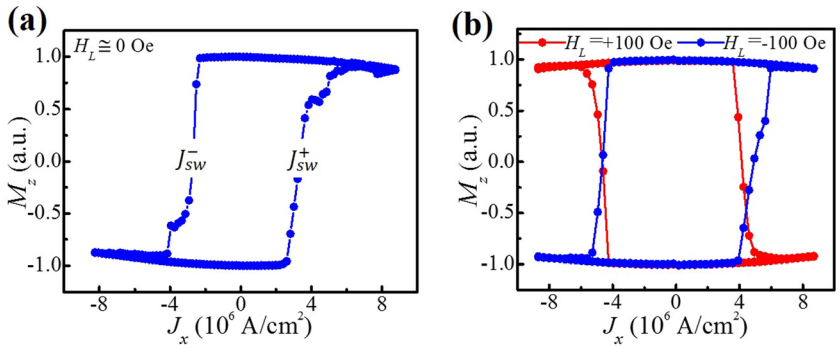

FIG. 4. Current-induced out-of-plane magnetization, M_z (normalized from EHE data) as a function of the current density for device I (Hf|CoFeB|MgO) without external magnetic field (a) and device II (Hf|CoFeB|TaO_x) under a longitudinal bias magnetic field, H_L (b). Note that reversing the direction of the bias field reverses the preferred switching directionality for magnetic-field-assisted switching, as expected.

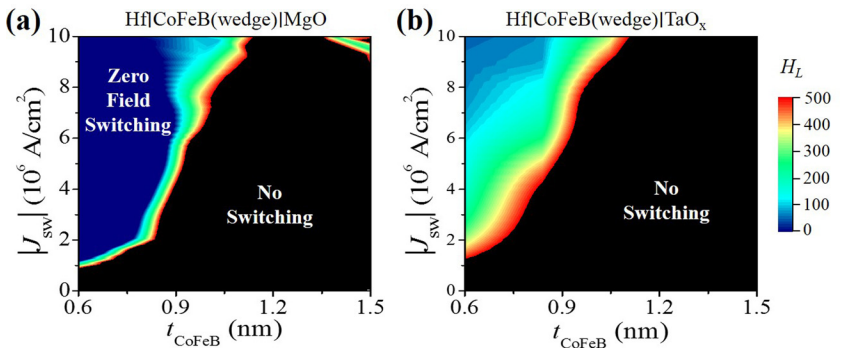

FIG. 5. Current-induced perpendicular magnetic switching phase diagram. (a) and (b) The switching current density $|J_{sw}|$ determined from $|(J_{SW}^+ - J_{SW}^-)|/2$, as a function of the CoFeB thickness in Hf|CoFeB(wedge)|MgO and Hf|CoFeB(wedge)|TaO_x, respectively. The color bar on the right side corresponds to the external magnetic field magnitude varying from 0 to 500 Oe. The black area denotes no full magnetic switching up to the experimental range of currents and bias fields.

4(a)) and under a constant longitudinal external magnetic field, H_L in Hf|CoFeB|TaO_x (Fig. 4(b)). It is observed that the perpendicular effective field, H_z^{FL}, allows for deterministic switching of the perpendicularly magnetized CoFeB layer, using an in-plane electric current without an external magnetic field in Hf|CoFeB|MgO (device I). However, in device II which is capped with TaO_x, an external magnetic field is necessary to switch the magnetization via in-plane currents due to the small β_z. This field, $H_L = \mp 100$ Oe, serves to tilt the magnetization from the z axis to enable deterministic switching of CoFeB.[20,21] We performed current-induced magnetic switching measurements for devices with different CoFeB thickness along the wedge. Based on the data, one can construct a phase diagram for current-induced magnetic switching in these samples, which is given in Fig. 5 for Hf|CoFeB(wedge)|MgO (a) and Hf|CoFeB(wedge)|TaO_x (b). In these figures, the switching current density was determined using $|J_{SW}| = |(J_{SW}^+ - J_{SW}^-)|/2$, where J_{SW}^+ (J_{SW}^-) is the positive (negative) switching current density (see Fig. 4(a)). The current-induced magnetic switching distributions are represented by color, which changes from blue ($|H_L| = 0$ Oe) to red ($|H_L| = 500$ Oe). The black color represents that there is no full magnetic switching within the applied range of current density (up to 10^7 A/cm^2) and longitudinal magnetic field (up to 500 Oe). The dark blue area represents zero-field magnetic switching in Fig. 5(a), indicating that below CoFeB thickness of ~0.9 nm, the perpendicularly magnetized CoFeB can be switched by current-induced torques at zero magnetic field. The switching current density increases with the CoFeB thickness as expected, because the PMA is increasing with the thickness in this range, while also the β_z magnitude is decreasing with increasing CoFeB thickness below 0.9 nm. On the other hand, in Fig. 5(b), one does not observe any current-driven magnetic switching at zero magnetic field within the present range of currents, as expected due to the very small β_z for all devices on the Hf|CoFeB(wedge)|TaO_x sample.

In conclusion, we have demonstrated the electric current-induced perpendicular magnetization switching, and its dependence on the choice of different oxide layers, in Hf|CoFeB(wedge)|(MgO or TaO_x) structures. To break the structural symmetry in the sample plane, a CoFeB layer with varying thickness is used. While a large current-induced effective field in the z direction is observed in Hf|CoFeB|MgO, this was not the case in Hf|CoFeB|TaO_x. It was also shown that the current-induced magnetic switching phase diagram in Hf|CoFeB(wedge)|(MgO or TaO_x) is in good agreement with the magnitude of β_z. Due to the high tunneling magneto-resistance ratio in MTJ devices with MgO barrier, a three-terminal MTJ device comprising Hf|CoFeB|MgO can potentially be used to manipulate the free layer in Magnetic Random Access Memory arrays, writing data using the current-induced SOT effect under zero magnetic field.

This work was partially supported by the NSF Nanosystems Engineering Research Center for Translational Applications of Nanoscale Multiferroic Systems (TANMS). This work was also supported in part by the FAME Center, one of six centers of STARnet, a Semiconductor Research Corporation (SRC) program sponsored by MARCO and DARPA. We would further like to acknowledge the collaboration of this research with King Abdul-Aziz City for Science and Technology (KACST) via The Center of Excellence for Green Nanotechnologies (CEGN). M.A.

This article is copyrighted as indicated in the article. Reuse of AIP content is subject to the terms at: http://scitation.aip.org/termsconditions. Downloaded to IP: 128.97.89.222 On: Fri, 22 May 2015 17:17:30

would like to acknowledge TÜBİTAK "*The Scientific and Technological Research Council of Turkey*" for his financial support during this work. This work was also partially supported by Cukurova University (Adana/Turkey) under the Project No. of 2013, FEF2013D31.

[1]L. Liu, C.-F. Pai, Y. Li, H. W. Tseng, D. C. Ralph, and R. A. Buhrman, Science **336**, 555 (2012).
[2]Z. Diao, Z. Li, S. Wang, Y. Ding, A. Panchula, E. Chen, L.-C. Wang, and Y. Huai, J. Phys.: Condens. Matter **19**, 165209 (2007).
[3]K. L. Wang, J. G. Alzate, and P. K. Amiri, J. Phys. D: Appl. Phys. **46**, 074003 (2013).
[4]J. C. Slonczewski, J. Magn. Magn. Mater. **159**, L1 (1996).
[5]L. Berger, Phys. Rev. B **54**, 9353 (1996).
[6]K. L. Wang, I. Ovchinnikov, F. Xiu, A. Khitun, and M. Bao, J. Nanosci. Nanotechnol. **11**, 306 (2011).
[7]M. D. Stiles and A. Zangwill, Phys. Rev. B **66**, 014407 (2002).
[8]J. E. Hirsch, Phys. Rev. Lett. **83**, 1834 (1999).
[9]J. Sinova, D. Culcer, Q. Niu, N. A. Sinitsyn, T. Jungwirth, and A. H. MacDonald, Phys. Rev. Lett. **92**, 126603 (2004).
[10]S. O. Valenzuela and M. Tinkham, Nature **442**, 176 (2006).
[11]X. Fan, J. Wu, Y. Chen, M. J. Jerry, H. Zhang, and J. Q. Xiao, Nat. Commun. **4**, 1799 (2013).
[12]M. I. Dyakonov and V. I. Perel, Phys. Lett. A **35**, 459 (1971).
[13]K. Junyeon, S. Jaivardhan, H. Masamitsu, Y. Michihiko, F. Shunsuke, S. Tetsuhiro, M. Seiji, and O. Hideo, Nat. Mater. **12**, 240 (2012).
[14]M. Akyol, J. G. Alzate, G. Yu, P. Upadhyaya, K. L. Wong, A. Ekicibil, P. Khalili Amiri, and K. L. Wang, Appl. Phys. Lett. **106**, 032406 (2015).
[15]G. Yu, P. Upadhyaya, Y. Fan, J. G. Alzate, W. Jiang, K. L. Wong, S. Takei, S. A. Bender, L.-T. Chang, Y. Jiang *et al.*, Nat. Nano **9**, 548 (2014).
[16]G. Yu, L.-T. Chang, M. Akyol, P. Upadhyaya, C. He, X. Li, K. L. Wong, P. K. Amiri, and K. L. Wang, Appl. Phys. Lett. **105**, 102411 (2014).
[17]C.-F. Pai, M.-H. Nguyen, C. Belvin, L. H. Vilela-Leão, D. C. Ralph, and R. A. Buhrman, Appl. Phys. Lett. **104**, 082407 (2014).
[18]G. Yu, P. Upadhyaya, K. L. Wong, W. Jiang, J. G. Alzate, J. Tang, P. K. Amiri, and K. L. Wang, Phys. Rev. B **89**, 104421 (2014).
[19]S. Emori, U. Bauer, S.-M. Ahn, E. Martinez, and G. S. D. Beach, Nat. Mater. **12**, 611 (2013).
[20]L. Liu, O. J. Lee, T. J. Gudmundsen, D. C. Ralph, and R. A. Buhrman, Phys. Rev. Lett. **109**, 096602 (2012).
[21]I. M. Miron, G. Gaudin, S. Auffret, B. Rodmacq, A. Schuhl, S. Pizzini, J. Vogel, and P. Gambardella, Nat. Mater. **9**, 230 (2010).

This article is copyrighted as indicated in the article. Reuse of AIP content is subject to the terms at: http://scitation.aip.org/termsconditions. Downloaded to IP: 128.97.89.222 On: Fri, 22 May 2015 17:17:30